ELSEVIER

15 July 1996

Optics Communications 128 (1996) 363–376

OPTICS COMMUNICATIONS

Full length article

Effect of the external cavity length in the dynamics of a semiconductor laser with optical feedback

C. Masoller

Instituto de Física, Facultad de Ciencias, Universidad de la República, Montevideo, Uruguay
Instituto de Física, Facultad de Ingeniería, Universidad de la República, Montevideo, Uruguay

Received 17 August 1995; revised version received 9 November 1995; accepted 8 December 1995

Abstract

The dynamics of a semiconductor laser with optical feedback is studied numerically for increasing time delay. Although the dimension of the attractors generally increases with the delay time, i.e., for short external cavities the attractor is a fixed point or a limit cycle, while for longer external cavities the attractor is a complicated torus or a chaotic attractor, special behavior is found when the external cavity length is chosen such that the product of the delay time τ with the relaxation oscillation frequency of the laser f_{rsol} yields a number close to integer. For these values of the time delay, the attractors become topologically simpler, i.e., in the regions where the attractor is a limit cycle, for $\tau f_{rsol} \approx n$ it becomes a fixed point, in the regions where is a two-torus, it becomes a limit cycle. Also, Lyapunov analysis indicates that in the resonance regions, the stability of the attractors changes strongly. The effects of the resonances are strong for short external cavities but become difficult to detect as the delay time increases.

PACS: 42.50.Lc; 05.45.+b

1. Introduction

The optical feedback in semiconductor lasers has attracted many researcher's attention owing to its practical importance as well as to the rich variety of nonlinear behavior. The basic properties of a semiconductor laser with weak optical feedback can be derived from simple rate equations for the complex electric field and carrier density proposed by Lang and Kobayashi [1]. The equations give a detailed understanding of the main characteristic features of the external cavity laser, such as the observed linewidth reduction, stability properties, noise properties and transition to coherence collapse [2–13]. In addition to its importance in many applications, the presence of delay intrinsically creates an infinite number of degrees of freedom, rending the external cavity coupled laser a good candidate for exploring low and high dimensional chaos in an infinite dimensional phase space.

In general, in time delayed systems, low-dimensional attractors arise for small delay, and on the contrary, in the long-delay limit, a more complex high-dimensional dynamics appears. Since time delayed dynamical systems appear in many physical situations, a lot of effort has been done to understand how the dynamics and the complexity of the attractors vary with the delay time τ. Farmer [14] studied the attractor of the Mackey-Glass equation, which is a model of blood production, and found that the Lyapunov spectra decreases as $1/\tau$, while the metric entropy converges to a finite value and the fractal

SSDI 0030-4018(95)00762-8

dimension increases linearly with τ. A similar linear growth of fractal dimension with space dimension was found in a partial differential equation [15]. Farmer's results were later confirmed by Ikeda and Matsumoto [16] who studied the Ikeda equation, which is a model of a nonlinear optical resonator. Also, Le Berre et al. [17], studying the attractors of a ring cavity delay optical system, found that the number of positive Lyapunov exponents and the Lyapunov dimension increase almost linearly with the delay time. Using statistical methods Dorizzi et al. [18] have shown that the dimension of the chaotic attractor of dissipative scalar-delay-differential equations in the case of periodic feedback is approximately equal to the number of times the smallest characteristic time is contained inside the delay.

In the Mackey-Glass equation and in the Ikeda equation, the nonlinear interactions are due only to the delayed feedback, i.e., are equations of the form $dx/dt = -ax + f(x-\tau)$. As was shown in Ref. [19] this equation becomes chaotic according to the Ruelle-Takens-Newhouse route. However, if a more general nonlinear local interaction is considered, the route to chaos is different, as shown by Arecchi et al. [20], who studied the dynamics of a CO_2 laser with feedback and showed that, in the short-delay regime, low dimensional chaos was reached by the destabilization of a two-dimensional torus (Curry-Yorke's route to chaos). In Ref. [21], high-dimensional chaos in dynamical systems with delayed feedback have been modeled with a general class of iterative delay maps and scaling laws of the Lyapunov spectra with a number of degrees of freedom have been found. Recently, a different approach to the study of delayed dynamical systems was presented in Ref. [22], where the fact that a delay dynamical system can be assimilated to a spatially extended system was used to study phase defects in a CO_2 laser with delayed feedback. The data was visualized by rearranging it in a two-dimensional representation, and the experimental findings were modeled via a generalized Landau equation with a delayed coupling.

In spite of the fact that the semiconductor laser coupled to an external cavity has been extensively studied by many authors, how the complexity of the attractors and the route to chaos vary with the delay time is not yet fully understood. The aim of the present paper is to study theoretically and by computer simulation, the effect of the external cavity length on the attractors of the system. In particular, we focus our study in situations where the external cavity is short enough to confine the dynamics in the low-dimensional region (stationary, periodic and quasi-periodic behavior). In a planned companion paper [23], we explore the opposite limit of long delay where the dynamics is highly chaotic.

Ye et al. [7] observed experimentally that, if the external cavity length was chosen such that the product of the delay time τ with the relaxation oscillation frequency of the solitary laser f_{rsol} yields an integer number, frequency locking occurs and instead of the usual quasi-periodic route, a period-doubling route to chaos appears as the feedback is increased. Also, Ritter and Haug [8] proved that depending on the value of τf_{rsol}, one or two coexisting limit cycles with different oscillation frequencies bifurcate from the same mode of the external cavity. When $\tau f_{rsol} \approx n$ (n integer), two sets of zeros of the system determinant $D(s)$ move into the right half s plane for almost the same value of the feedback intensity k, resulting in the coexistence of two periodic attractors originated from the same mode. Their result is in agreement with the numerical and experimental findings of Mørk et al. [5].

With the motivation of these experimental observations, the main question we want to answer is: are there special values of the external cavity length, i.e., particular values of the delay time, such that the laser presents special behavior? And also, how does the complexity of the dynamics depend on the delay time? Our analysis, while confirming the conjecture of low-dimensional attractors for short delay time, and a more complex high-dimensional dynamics for long τ, reveals novel features too. We find that, as the length of the external cavity is augmented, i.e., the delay time τ increases, the laser follows a quasi-periodic route and the attractors become generally more complicated. However, the main difference with the usual quasi-periodic route is that for values of τ such that $\tau f_{rsol} \approx n$, the attractors reverse the chaotic route and become topologically simpler. This means that embedded in the periodic regime, i.e., in the region of the delay time such that the attractor is a limit cycle, are stationary regions where the attractor undergoes an inverse Hopf bifurcation and becomes a fixed point again. Embedded in the quasi-

periodic regime, i.e., in the region of the delay time that the attractor is a two-torus, are periodic regions where the attractor undergoes an inverse Hopf bifurcation and becomes a limit cycle again. Also, for even higher values of τ, the two-torus undergoes a sequence of period-doubling and inverse period-doubling bifurcations before becoming chaotic.

Lyapunov analysis reveals that the Lyapunov exponents present a particular behavior for those values of τ satisfying $\tau f_{\mathrm{rsol}} \approx n$, which indicates that not only the topology, but also the stability of the attractor changes strongly in the resonances. We also find that, in most of the resonance regions, the largest (negative) Lyapunov exponents have a local minimum and thus the dynamics of the laser is more stable for these particular values of the external cavity length.

The resonance regions found when the delay time is varied have not been reported previously to our knowledge, and besides their theoretical interest, these regions might have practical importance, since a stabilized regime of operation is essential in order to satisfy the requirements of many applications where semiconductor lasers operate in the presence of external optical feedback, such as optical data recording and fiber optic communication systems. However, from Fig. 5b of Ref. [5] is clear that, as τ increases from $\tau f_{\mathrm{rsol}} = n$ to $\tau f_{\mathrm{rsol}} = n + 1$, for suitable values of the feedback level k and $n < n_{\max}$ (where $n_{\max}$ depends on k), the attractor will pass two Hopf bifurcation boundaries and thus it will bifurcate from a fixed point to a limit cycle and then back again to a fixed point.

Finally, let us mention that the behavior in the resonance regions found might be originated by a nonlinear interaction between the external cavity modes (separated by a frequency $f_{\mathrm{ext}} = 1/\tau$) and the relaxation oscillation frequency f_{rsol} of the solitary laser. It is well known that the cavity formed by the external feedback introduces a series of resonant frequencies in the laser, and that the competition and interplay between these natural frequencies that arises as the feedback level is increased is the cause of successive instabilities that give rise to chaotic behavior. Several different chaotic transitions have been reported numerically and experimentally, but the most common one is the quasiperiodic route in which the relaxation oscillation and the external cavity frequencies occur sequentially and are incommensurate. In the periodic resonance regions embedded in the quasi-periodic regime, under the resonance condition $\tau f_{\mathrm{rsol}} = n$, the frequencies f_{ext} and f_{rsol} become commensurate and the two-torus turns into a limit cycle. This limit cycle follows the period-doubling route observed experimentally in Ref. [7] as the feedback in increased.

This paper is organized as follows. In Section 2 a brief description of the theoretical model of Lang and Kobayashi for the external cavity-coupled laser is given. The bifurcation diagram of the external cavity modes of the laser, i.e., the fixed points of the systems, as the delay time increases is discussed. Section 3 presents the numerical results, and Section 4 contains the discussion and conclusions.

2. Theory

The dynamical properties of external cavity lasers are usually described with the Lang and Kobayashi rate equations [1] for the amplitude $E_0(t)$ and the phase $\phi(t)$ of the electric field and the average carrier density $N(t)$ in the active region

$$\frac{\mathrm{d}E_0(t)}{\mathrm{d}t} = \tfrac{1}{2}\left[G(N) - 1/\tau_{\mathrm{p}}\right] E_0(t) + \frac{k}{\tau_{\mathrm{in}}} E_0(t-\tau)\cos\left[\Delta(t)\right], \tag{1}$$

$$\frac{\mathrm{d}\phi(t)}{\mathrm{d}t} = \tfrac{1}{2}\alpha\left[G(N) - 1/\tau_{\mathrm{p}}\right] - \frac{k}{\tau_{\mathrm{in}}}\frac{E_0(t-\tau)}{E_0(t)}\sin\left[\Delta(t)\right], \tag{2}$$

$$\frac{\mathrm{d}N(t)}{\mathrm{d}t} = J - \frac{N(t)}{\tau_{\mathrm{s}}} - G(N)\,E_0(t)^2. \tag{3}$$

In these equations the field amplitude $E_0(t)$ is normalized such that $V_{\mathrm{c}} E_0(t)^2$ is the total photon number in the laser waveguide (where V_{c} is the volume of the active region). τ is the delay time ($\tau = 2L/c$ where L is the length of the optical path and c is the velocity of light), τ_{s} is the carrier lifetime or population inversion lifetime, τ_{p} is the photon lifetime and τ_{in} is the round-trip time in the laser cavity. $\Delta(t) = \omega_0\tau + \phi(t) - \phi(t-\tau)$ is the phase delay (where ω_0 is the laser frequency without feedback at the threshold of the laser operation). The

linear gain per unit time is $G(N) = g(N - N_0)$ with g being the modal gain coefficient and N_0 the carrier density at transparency. k is the feedback parameter, i.e., k^2 is the power reflected from the external cavity relative to the power reflected from the laser mirror. α is the linewidth enhancement factor and J is the current density in carriers per unit volume and unit time.

Eqs. (1)–(3) take into account only a single feedback term, thus their validity is limited to weak to moderated feedback levels ($k \ll 1$). We omit the quantum noise terms that take into account the spontaneous recombination effects. As it is well known, these can be neglected for moderate optical feedback when compared to the feedback terms.

The stationary solutions of Eqs. (1)–(3) are the external cavity modes (ECM) of the laser and can be written as $E_0(t) = E_S$, $\phi(t) = (\omega_S - \omega_0)t$, $N(t) = N_S$. The angular frequencies ω_S are easily obtained from the phase condition [2]

$$f(\omega) = \omega - \omega_0 + (k/\tau_{in})(\alpha \cos \omega\tau + \sin \omega\tau) = 0, \quad (4)$$

which may have multiple solutions, corresponding to multiple external cavity modes. The carrier density and field amplitude of a given ECM are

$$N_s = N_{th} - 2\frac{k}{g\tau_{in}}\cos \omega_s\tau, \quad (5)$$

$$E_s^2 = \frac{J - N_s/\tau_s}{g(N_s - N_0)}. \quad (6)$$

The solutions of (4) can be graphically obtained as shown in Fig. 1. Since the amplitude of the sine and cosine terms in (4) depends on k, and the period depends on τ, the number of solutions increases as the value of k or τ increases. The value of $C = k\tau/\tau_{in}\sqrt{1+\alpha^2}$ determines the number of modes [3,5]. For $C < 1$ only one mode exists, which can be identified as the laser cavity mode perturbed by the external cavity. For $C > 1$ three or more modes exist, each of which can be identified as a perturbed external mode. In the limit $C \gg 1$ the total number of modes is approximately given by $C/\pi + 1$ [5].

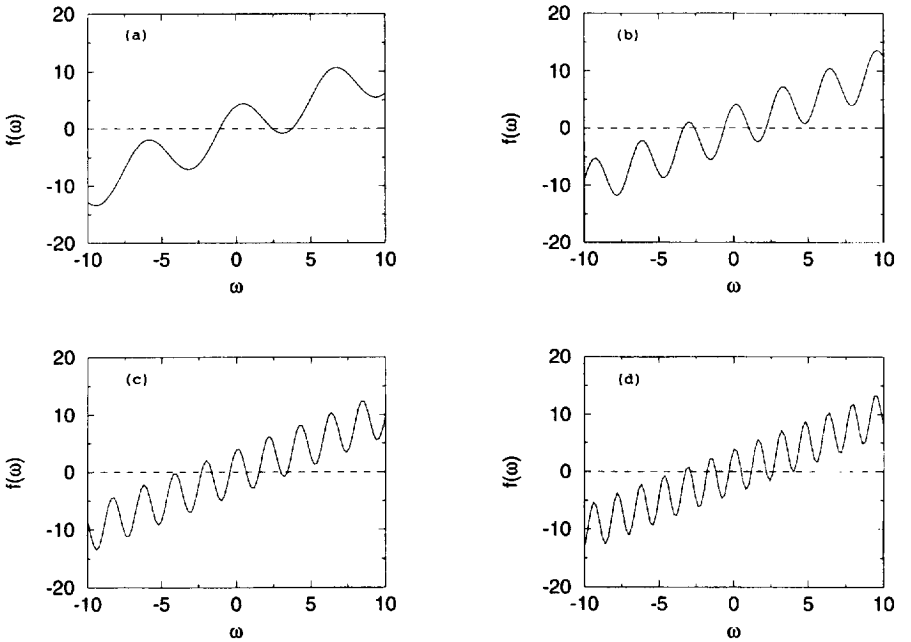

Fig. 1. Graphical solution for the phase condition (4) for $\omega_0\tau \bmod(2\pi) = 0$, $\alpha = 4.4$, $k = 0.006$ and (a) $\tau = 1$ ns; (b) $\tau = 2$ ns; (c) $\tau = 3$ ns; (d) $\tau = 4$ ns.

From Eqs. (4) and (5), the fixed point solutions lie on the circumference

$$\left[\omega_s - \omega_0 - \frac{1}{2}\alpha\, g(N_s - N_{th})\right]^2 + \left[\frac{1}{2} g(N_s - N_{th})\right]^2 = k^2/\tau_{in}{}^2. \quad (7)$$

Fig. 2 shows the position of the fixed points in the circumference, for fixed k and an increasing value of τ.

The stability of the fixed points is determined by the position of the zeros of the system determinant $D(s)$. A linear stability analysis shows that as k or τ increase, the fixed points are created in pairs by saddle-node bifurcations: one fixed point is initially stable (mode) while the other is always unstable (antimode). If

$$\frac{d\omega_0}{d\omega} = 1 + \frac{k\tau}{\tau_{in}}[-\alpha \sin(\omega\tau) + \cos(\omega\tau)] < 0 \quad (8)$$

for $\omega = \omega_S$, the determinant $D(s)$ has a zero on the real axis in the right half s plane [2], i.e., the corresponding ECM is an antimode. Thus, according to (8), the antimodes are the graphical solutions in Fig. 1 where the sinusoidal curve is decreasing with ω. The stability boundary (8) can be rewritten as

$$y = \alpha x + 1/\tau, \quad (9)$$

where $x = \omega - \omega_0 - \alpha\, g(N - N_{th})/2$ and $y = g(N - N_{th})/2$. In Fig 2, the solutions to the left of (9) (shown as a dashed line) are the antimodes.

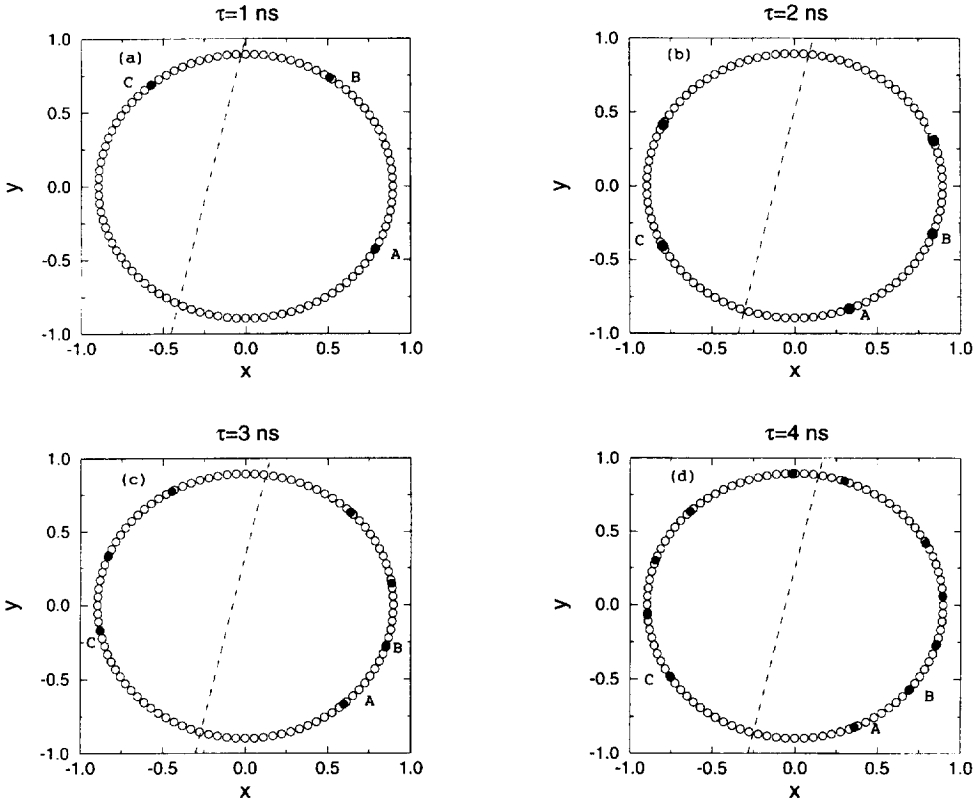

Fig. 2. Modes and antimodes in the (x, y) plane, where $x = \omega - \omega_0 - \alpha\, g(N - N_{th})/2$ and $y = g(N - N_{th})/2$. The circumference (7) is shown with empty circles, the solutions of (4) with filled circles, and the stability boundary (9) with dashed line. The parameter values are the same of Fig. 1. (a) $\tau = 1$ ns; (b) $\tau = 2$ ns; (c) $\tau = 3$ ns; (d) $\tau = 4$ ns.

Since the number of ECM depend on the value of $C = k\tau/\tau_{in}\sqrt{1+\alpha^2}$, the number of modes and anti-modes in the circumference (7) increases linearly with the delay time but since the size of the circumference does not increase, the modes approach each other becoming more dense in the circumference (see Fig. 2). On the contrary, when k increases for fixed τ, both, the number of modes and the size of the circumference increase, and thus, the density of modes in the circumference does not vary (see, e.g., Ref. [5], Fig. 4). Interestingly, in both cases, the value of $\omega_S\tau$ of each mode converges to a constant value in the limit of large k or τ (see Fig. 3 for constant k and increasing τ, and Ref. [10], Fig. 1b for constant τ and increasing k).

In Ref. [10] the coexistence of attractors was studied for an increasing value of k and a fixed value of τ. It was found that all the initially stable modes, that are created thus direct saddle-node bifurcations as k increases, undergo Hopf bifurcations and turn into a limit cycle first, and then into a two-torus. The following evolution of the two-torus depends on parameter values and on the fixed point that originated the attractor, i.e., it could turn into a three-torus, it could period double, or it could turn directly into a strange attractor. Since the number of fixed points depend on the product $k\tau$, and the stability condition (8) also depends on the value of $k\tau$, we might expect a similar route to chaos if instead of increasing k for a fixed value of τ, we increase τ for a fixed value of k. This is true in the sense that in both cases, the laser follows a quasi-periodic route to chaos. However, in the next section we will show that in the second case there are special regions of the parameter τ in which the attractor reverses the route to chaos, i.e., if the attractor is a limit cycle it becomes a fixed point; if is a two-torus it becomes a limit cycle; if is a two-torus that period doubled it undergoes an inverse period-doubling bifurcation and becomes a simple two-torus again.

3. Results

The values adopted for the parameters in the numerical simulation are: $k = 0.006$, $\alpha = 4.4$, $g = 1.1 \times 10^{-12}$ m^3/s, $N_0 = 1.1 \times 10^{24}$ m^{-3}, $\omega_0\tau \times \mathrm{mod}(2\pi) = 0$, $\tau_S = 2$ ns, $\tau_p = 2$ ps, $\tau_{in} = 6.7$ ps. J was taken as $J = 2.0J_{th}$, where J_{th} is the threshold current density. Finally, the delay time τ is taken as control parameter, which is varied to study the behavior of the laser.

In order to follow the evolution of the attractors

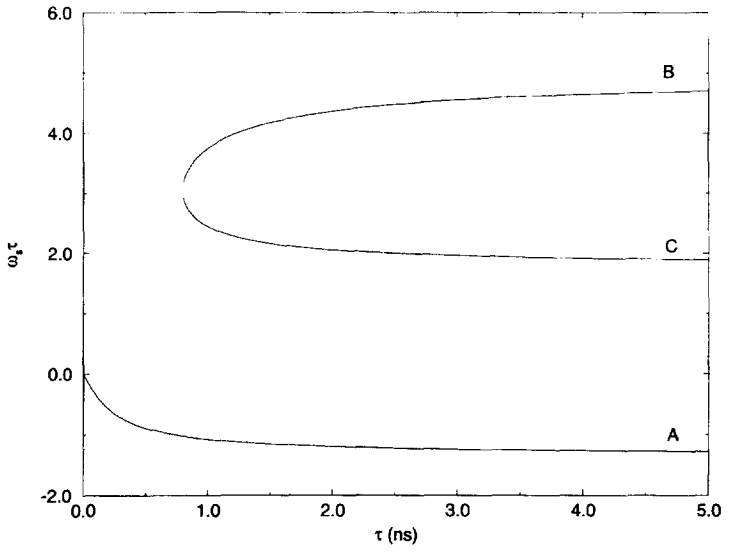

Fig. 3. $\omega_s\tau$ as a function of τ, for the modes labeled A, B and C in Fig. 2. Notice that, as τ increases, althought the modes become more dense and approach each other in the circumference (7), the value of $\omega_s\tau$ converges to a constant value as τ increases.

originated from the initially stable modes of the laser for increasing values of τ, Eqs. (1)–(3) were solved directly using a Runge-Kutta method with a time increment $\Delta t = 1$ps and the initial conditions were taken from Eqs. (4)–(6). For simple attractors, i.e. fixed point or limit cycles, we visualized the dynamics projecting the trajectory (after a certain number of round trips in order to eliminate transient effects) in the plane formed by the normalized intensity $(I(t)/I_{sol} = E(t)^2/E_{sol}^2)$ and the phase difference $(\phi(t) - \phi(t-\tau))$. When the attractor becomes more complicated, i.e., a two torus or a chaotic attractor, to visualize the dynamics we used the Poincaré section technique [24]. We calculated the intersection of the trajectory with the plane $I(t)/I_{sol} = 1$ and plotted the section in the plane formed by the normalized carrier density $(N/N_{th} - 1)$ and the phase difference $(\phi(t) - \phi(t-\tau))$. In order to be able to compare the sizes of the attractors, all graphs are done with the same axes and scales.

We study the stability of the attractors originated from the external cavity modes of the laser using the Lyapunov exponents technique. The positive (negative) exponents measure average exponential divergence (convergence) of nearby trajectories, onto the phase-space attractor. Since the laser diode with feedback from an external cavity is a system with infinite dimensions, to calculate the Lyapunov exponents we use Farmer's method [14] and study the evolution of infinitesimal perturbations that are vectors with three components, two of which (the field and the amplitude) are functions of time over the entire delay τ [10].

Fig. 4 shows some typical Poincaré sections of the attractor originated from the perturbed laser cavity mode for increasing values of τ (following the notation of Ref. [10], we will refer to this attractor as attractor A). Several different regimes of operation can be distinguished. The interval $0 < \tau < 0.29$ ns corresponds to the stationary region, where the attractor is a fixed point, i.e., the laser operates in the stable perturbed laser cavity mode. At $\tau = 0.29$ ns a Hopf bifurcation occurs and a limit cycle emerges (its Poincaré section is the point indicated with a

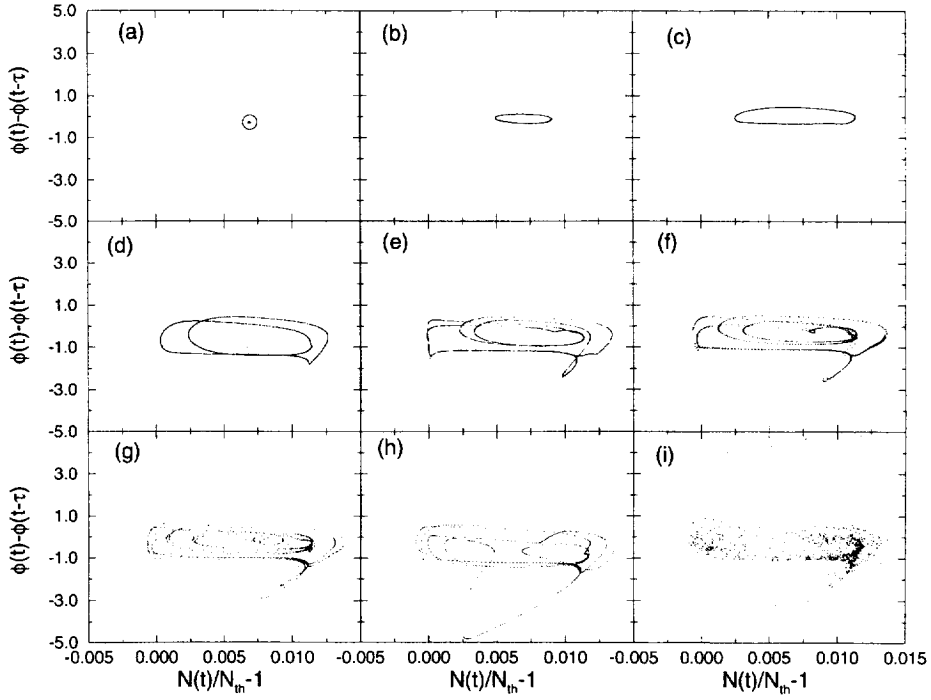

Fig. 4. Poincaré section of attractor A for (a) τ = 1.2 ns; (b) 1.4 ns; (c) 2.0 ns; (d) 3.0 ns; (e) 3.4 ns; (f) 3.6 ns; (g) 3.8 ns; (h) 5.4 ns; (i) 5.5 ns.

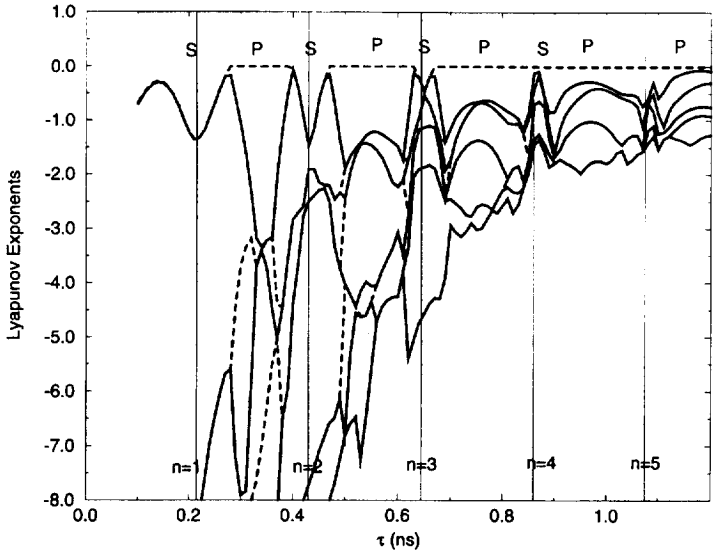

Fig. 5. Eight largest Lyapunov exponents of attractor A for $0 < \tau < 1.2$ ns. λ_1, λ_3, λ_5, λ_7 are plotted with dashed lines while λ_2, λ_4, λ_6, λ_8 are plotted with solid lines. The regions labeled with P are the periodic regions ($\lambda_1 = 0$, λ_2, λ_3, $\lambda_4 \ldots < 0$) while the regions labeled with S are the stationary regions (λ_1, λ_2, $\lambda_3 \ldots < 0$). The values of τ that satisfy $\tau f_{\mathrm{rsol}} = n$ are indicated with vertical lines.

circle in Fig. 4a). The interval 0.29 ns $< \tau <$ 1.35 ns corresponds to the periodic region, where undamping of the relaxation oscillations occurs. A secondary Hopf bifurcation occurs at $\tau = 1.35$ ns and a two-torus appears. The interval 1.35 ns $< \tau <$ 5.5 ns corresponds to the quasiperiodic region, in which the excitation of the external cavity modes occur. The Poincaré section of the torus is shown in Figs. 4b and 4c. The torus period-doubles a few times (Figs. 4d, 4e, 4f 4g) and its Poincaré section becomes very

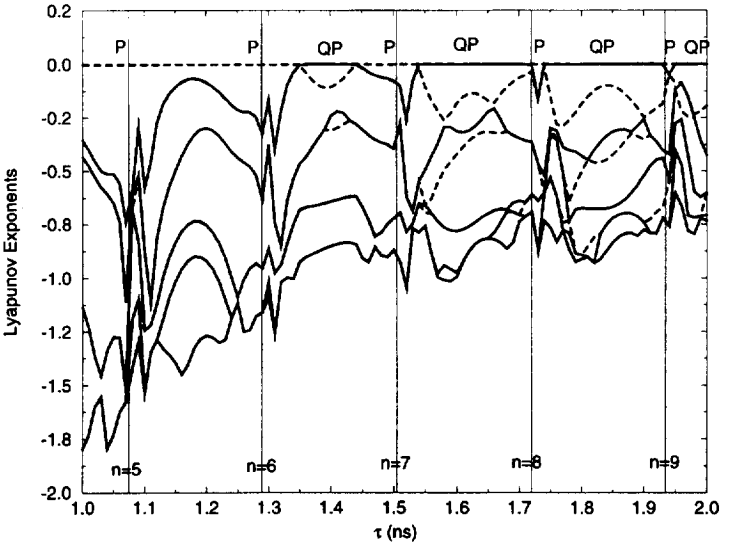

Fig. 6. Eight largest Lyapunov exponents of attractor A for 1 ns $< \tau <$ 2 ns. λ_1, λ_3, λ_5, λ_7 are plotted with dashed lines while λ_2, λ_4, λ_6, λ_8 are plotted with solid lines. The regions labeled with P are the periodic regions ($\lambda_1 = 0$, λ_2, λ_3, $\lambda_4 \ldots < 0$) while the regions labeled with QP are the quasi-periodic regions (λ_1, $\lambda_2 = 0$, λ_3, $\lambda_4 \ldots < 0$). The values of τ that satisfy $\tau f_{\mathrm{rsol}} = n$ are indicated with vertical lines.

complicated (Fig. 4h). For higher values of τ, the torus becomes unstable and the trajectory evolves chaotically between attractor A and the attractor originated from the compound cavity mode B of Fig. 3 (see Fig. 4i).

To gain insight into the main features of the dynamics, we study in more detail the evolution of attractor A for short delays, i.e., before the first period-doubling bifurcation of the two-torus occurs. Figs. 5 and 6 show the eight largest Lyapunov exponents of the attractor for increasing values of τ (Fig. 5 shows the exponents in the region $0 < \tau < 1.2$ ns, before the two-torus appears, while Fig. 6 shows the exponents in the region 1.0 ns $< \tau <$ 2 ns, before the first period doubling bifurcation occurs). Since the Lyapunov exponents are the real part of complex eigenvalues, there are regions of τ in which couples of exponents have the same value and this is the reason why in the figures we cannot distinguish eight different lines. In order to facilitate the interpretation of the results, we have plotted λ_1, λ_3, λ_5, λ_7 with dashed lines and λ_2, λ_4, λ_6, λ_8 with solid lines.

Figs. 5 and 6 clearly show the special behavior of the Lyapunov exponents for values of the delay time such that $\tau f_{\mathrm{rsol}} \approx n$, n integer and f_{rsol} being the relaxation oscillation frequency of the solitary laser (the values of τ that satisfy $\tau f_{\mathrm{rsol}} = n$ are indicated with vertical lines).

In Fig. 5 we can see that in the stationary region (for $0 < \tau < 0.29$ ns) the attractor is a fixed point that has all his Lyapunov exponents less than zero. At $\tau = 0.29$ ns, when λ_1 becomes zero, a Hopf bifurcation occurs and a limit cycle is created. For values of the time delay 0.29 ns $< \tau <$ 1.35 ns there are stationary regions (labeled with S in Fig. 5) embedded in the periodic region (labeled with P). In the stationary regions λ_1 becomes negative again and the attractor is a fixed point while in the periodic regions, $\lambda_1 = 0$ (dashed line in Fig. 5) and the attractor is a limit cycle.

Typical attractors in each region are shown in Fig. 7 (the circles indicate the fixed points in the stationary regions, while the solid lines show the limit cycles in the periodic regions). In the first stationary

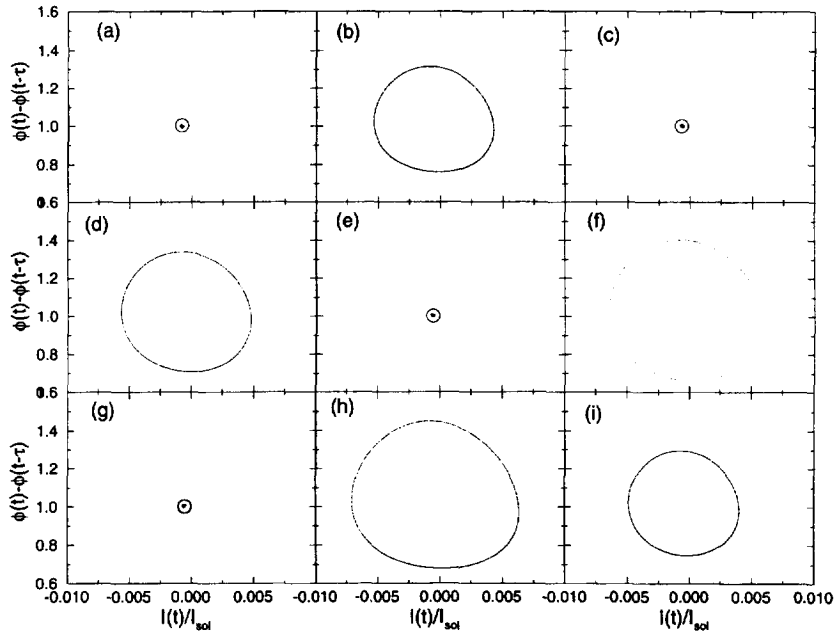

Fig. 7. Attractor A in the stationary and periodic regions of Fig. 5. After transients have died away, the trajectory is projected in the plane $I(t)/I_{\mathrm{sol}}$, $\phi(t) - \phi(t-\tau)$. (a) $\tau = 0.27$ ns; (b) 0.38 ns; (c) 0.43 ns; (d) 0.49 ns; (e) 0.66 ns; (f) 0.7 ns; (g) 0.87 ns; (h) 1.07 ns; (i) 1.082 ns.

region, for $\tau = 0.27$ ns (Fig. 7a), the fixed point has not become unstable yet; for $\tau = 0.38$ ns (Fig. 7b), the fixed point turned into a limit cycle. Figs. 7c, 7e, and 7g show the fixed point in the resonance stationary regions corresponding to $n = 2$, 3, and 4. Figs. 7d, 7f and 7h show the limit cycle in between the stationary regions. Notice that in the resonance corresponding to $n = 5$ we do not find the fixed point but instead the attractor is a limit cycle whose amplitude is slightly smaller that the amplitude of the limit cycles in the surrounding periodic regions (see Fig. 7i).

The spectrum of Lyapunov exponents of Fig. 6 shows that at $\tau = 1.35$ ns another Hopf bifurcation occurs when λ_2 becomes zero, and a two-torus is created. For values of the time delay 1.35 ns $< \tau <$ 2 ns there are periodic regions (labeled with P in Fig. 6) embedded in the quasi-periodic region (labeled with QP). In the period regions $\lambda_1 = 0$ (dashed line in Fig. 3), λ_2, λ_3, $\lambda_4 \ldots < 0$ and the attractor is a limit cycle, while in the quasi-periodic regions λ_1,$\lambda_2 = 0$ (solid line), λ_3, $\lambda_4 \ldots < 0$ and the attractor is a two-torus.

Typical Poincaré sections of the attractors in the periodic and quasi-periodic regions are shown in Fig. 8 (the circles indicate the limit cycles in the periodic regions, while the solid lines show the two-torus in the quasi-periodic regions). For $\tau = 1.30$ ns (Fig. 8a), the limit cycle has not become unstable yet; for $\tau = 1.37$ ns and 1.43 ns (Figs. 8b and 8c), the limit cycle turned into a two-torus. Figs. 8d, 8f, and 8h show the limit cycle in the resonance periodic regions corresponding to $n = 7$, 8, 9. Figs. 8e, 8g and 8i show the two-torus in between the periodic regime.

Also, if we study in detail the following evolution of the two-torus after the first period-doubling bifurcation, we find that it also presents the same kind of alternating behavior as the time delay increases: it undergoes the series of period-doubling and inverse period-doubling bifurcations, shown in Fig. 9.

The sequence of direct and inverse bifurcations shown in Figs. 7, 8 and 9 quite unexpected for us, has not been reported previously to our knowledge in any delay differential dynamical system, and is the main result of this paper.

The special behavior of the Lyapunov exponents

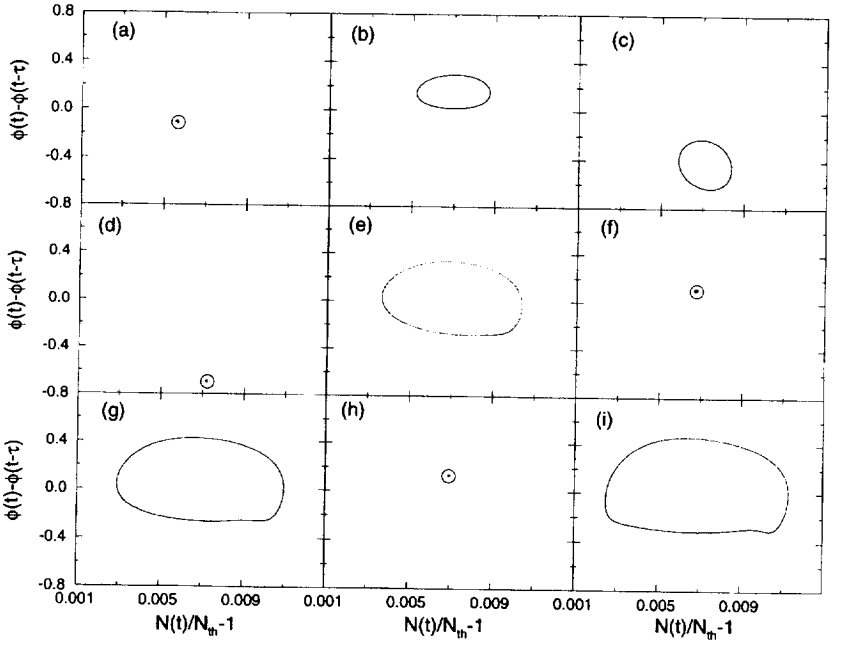

Fig. 8. Poincaré section of attractor A in the periodic and quasi-periodic regions of Fig. 6 (the Poincaré section is obtained intersecting the trajectory with the plane $I(t)/I_{sol} = 1$). (a) $\tau = 1.3$ ns; (b) 1.37 ns; (c) 1.43 ns; (d) 1.45 ns; (e) 1.6 ns; (f) 1.73 ns; (g) 1.80 ns; (h) 1.94 ns; (i) 2.0 ns.

in the regions where the delay time satisfies $\tau f_{rsol} \approx n$ indicates that in these regions, not only the topological structure of the attractor changes abruptly, but also its stability.

In the first resonance ($\tau f_{rsol} = 1$), which occurs in the stationary regime where the relaxation oscillations have not become undamped yet, the largest negative exponents of the fixed point (λ_1 and λ_2) present a local minimum. In the stationary regions embedded in the periodic regime, close to values that satisfy $\tau f_{rsol} = n$ ($n = 2$ and 3), a similar behavior is found: λ_1 and λ_2 present a local minimum, indicating stronger convergence towards the fixed point, i.e., the regime of operation is more stable for these values of the delay time. As was discussed in the introduction, these results are not only of theoretical interest buy might also have practical importance in technological applications where the laser operates in the presence of feedback, and the undamping of the relaxation oscillations should be avoided.

Contrarily, in the next three resonances ($n = 4$, 5, and 6), the attractor becomes barely stable, as its relevant exponents become almost zero. In the following resonances ($n = 7$, 8 and 9) corresponding to the periodic regions embedded in the quasiperiodic regime, again we encounter the same behavior: the attractor becomes more stable since λ_2 and λ_3 present a local minimum. The effect of the resonances in the value of the Lyapunov exponents is stronger for short delay, and becomes more difficult to detect as the time delay increases. Also, the size of the resonance region is larger for short delay and decreases as the delay time increases.

Since the stability and the topological properties of the attractors change abruptly between the stationary and periodic regions, one might ask the following questions: how are the fixed points of the stationary regions related to the limit cycles of the periodic regions? Are they originated from the same mode of the laser, or on the contrary, in the stationary regions

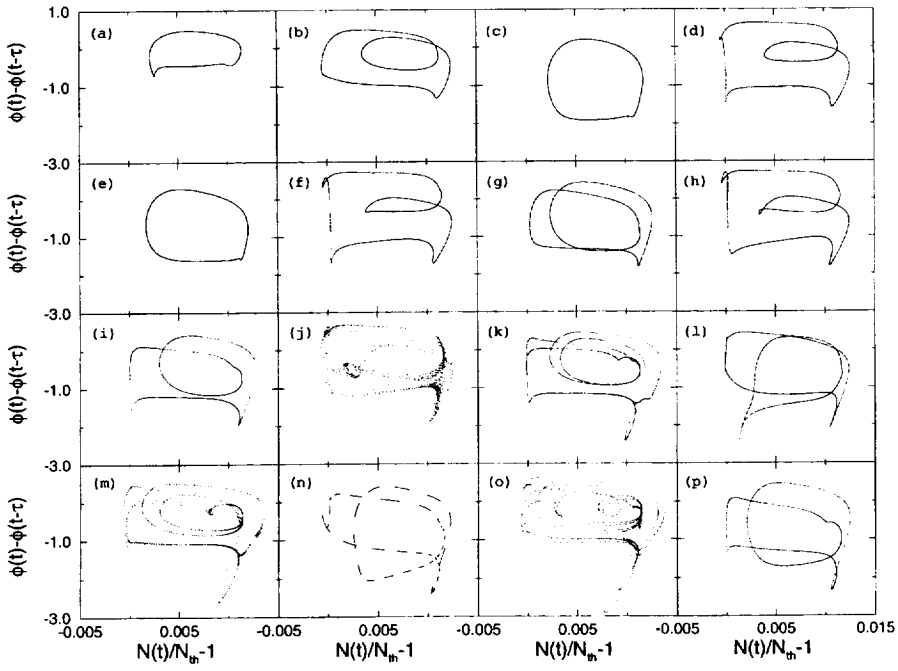

Fig. 9. Sequence of period-doubling and inverse period-doubling bifurcations that undergoes attractor A before becoming chaotic. The Poincaré section of the attractor is obtained intersecting the trajectory with the plane $I(t)/I_{sol} = 1$. (a) $\tau = 2.4$ ns; (b) 2.5 ns; (c) 2.6 ns; (d) 2.7 ns; (e) 2.8 ns; (f) 2.9 ns; (g) 3.0 ns; (h) 3.1 ns; (i) 3.2 ns; (j) 3.3 ns; (k) 3.4 ns; (l) 3.5 ns; (m) 3.6 ns; (n) 3.7 ns; (o) 3.8 ns; (p) 3.9 ns.

the limit cycle becomes unstable and the laser jumps to another attractor, possibly originated from another mode of the laser? In order to answer these questions, we studied the position and relaxation frequency of the attractors in both regions.

First, we compared the numerically calculated position of fixed points in the stationary regions (integrating Eqs. (1)–(3)) with the position of the perturbed laser mode (calculated analytically from Eqs. (4)–(6)) and an excellent agreement was found. Second, we compared the relaxation frequency to the fixed points in the stationary regions and the frequency of the limit cycles in the periodic regions with the onset angular frequency of the limit cycle, that can be analytically calculated from the equation [2]

$$\Omega^2 - \omega_r^2 = \Omega \cot(\Omega\tau/2)\left(1/\tau_s + \tau_p\omega_r^2\right), \qquad (10)$$

ω_r being the relaxation oscillation angular frequency of the solitary laser ($\omega_r = 2\pi f_{rsol} = \sqrt{gE_{sol}^2/\tau_p}$). Several possible solutions actually arise from Eq. (10) for fixed τ. In Fig. 10, we have plotted these solutions (with circles), together with the numerically calculated frequency of the limit cycle and the relaxation frequency to the fixed point (with solid dots), as a function of τ. A good agreement is found between the numerical and analytical results. However, since the solutions of (10) give the onset angular frequency of the limit cycle, i.e., the angular frequency of the limit cycle when born, the numerical results cannot match well with the solutions of (10) in the region where the fixed point has not become unstable yet ($\tau < 0.29$ ns). Also, it is interesting to notice that the stationary regions are centered around the values of τ such that the solution of Eq. (10) changes abruptly. A similar behavior was found in Ref. [11] (see Ref. [11], Fig. 11) under a short delay. The authors explain the results using a model of a two-resonator coupled system, since for low values of τ, the second cavity mode has little effect on the relaxation oscillation compared with the first and the system can be viewed as a two-resonator coupled system. When $\tau f_{rsol} = 1$ the system behaves as a coupled cavity with two identical resonance frequencies and thus, a slight increase of the delay time will swap the roles of the relaxation oscillation and the first ECM.

From the study of the position and relaxation frequency of the fixed points and limit cycles we can conclude that in the stationary regions the laser does not jump to another attractor (originated from another ECM) but on the contrary, the attractor corresponds to the same fixed point that originates the

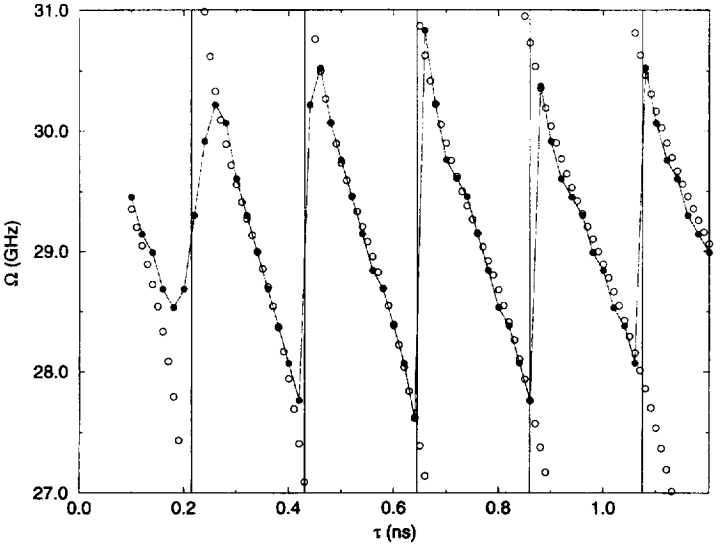

Fig. 10. Relaxation oscillation angular frequency as a function of the delay time. The circles represent the solutions of Eq. (10), obtained after some numerical procedures while the solid dots represent the values obtained from the numerical simulation.

limit cycle of the periodic regions, i.e., the attractor reverses the quasi-periodic route, undergoes an inverse Hopf bifurcation and becomes a fixed point again.

Finally, let us mention that the alternating behavior found in the attractor originated from the perturbed laser mode is also found in the attractor originated from the compound cavity mode B of Fig. 3, although it is more difficult to detect since this mode appears for higher values of τ.

4. Conclusions

In this paper we have studied in detail the evolution of the attractors of a semiconductor laser with optical feedback, as the time delay increases, i.e., as the length of the external cavity augments. We find that although the attractors follow a quasi-periodic route to chaotic behavior, they "reverse" the route for values of τ that satisfy the relationship $\tau f_{\mathrm{rsol}} \approx n$. For these values of the delay time, we find two interesting results.

First, in the resonance regions the attractor undergoes an inverse bifurcation and becomes topologically simpler. For short delay time we find Hopf and inverse Hopf bifurcations between a fixed point and a limit cycle (Fig. 7). For higher values of τ, Hopf and inverse Hopf bifurcations between a limit cycle and a two-torus (Fig. 8). For even higher values of τ, period-doubling and inverse period-doubling of the two-torus (Fig. 9).

Second, the Lyapunov exponents show that the stability of the attractor changes strongly when $\tau f_{\mathrm{rsol}} \approx n$. In most of the resonance regions the relevant exponents have a local minimum, indicating faster convergence towards the attractor, i.e., a more stable regime of operation. However, there are also a few resonances where the relevant exponents are almost zero, indicating that the attractor is marginally stable.

Physically, the resonance regions found can be considered to be the result of complex interaction among the compound cavity modes and the relaxation oscillation of the solitary laser. For example, the existence of periodic regions embedded in the quasiperiodic regime can be explained by the fact that under the resonance condition $\tau f_{\mathrm{rsol}} = n$, the frequencies f_{ext} and f_{rsol} become commensurate and the two-torus turns into a limit cycle. This interaction has already been reported to be the origin of the observed experimentally period-doubling route that occurs as the feedback level is increased and the relationship $\tau f_{\mathrm{rsol}} = n$ is maintained [7]. Also, when τ increases for a fixed value of k, a sequence of direct and inverse Hopf bifurcations between a fixed point and a limit cycle, can be deduced from Fig. 5b of Ref. [5]. However, which is the mechanism generally responsible for the alternating sequence of direct and inverse bifurcations found, is a very interesting question which deserves further study.

Acknowledgements

This work was supported by the Project 47 of the BID-CONICYT Program of the Consejo Nacional de Ciencia y Tecnologia (CONICYT) of Uruguay, the Comision Sectorial de Investigacion Cientifica (CSIC) and the PEDECIBA.

References

[1] R. Lang and K. Kobayashi, IEEE J. Quantum Electron. QE-16 (1980) 347.
[2] B. Tromborg, J.H. Osmundsen and H. Olesen, IEEE J. Quantum Electron. QE-20 (1984) 1023.
[3] G.A. Acket, D. Lenstra, A.J. den Boef and B.H. Verbeek, IEEE J. Quantum Electron. QE-20 (1984) 1163.
[4] J. Sacher, W. Elsässer and E.O. Göbel, Phys. Rev. Lett. 63 (1989) 2224.
[5] J. Mørk, J. Mark and B. Tromborg, Phys. Rev. Lett. 65 (1990) 1999;
J. Mørk, B. Tromborg and J. Mark, IEEE J. Quantum Electron QE-28 (1992) 93.
[6] J. Sacher, D. Baums, P. Panknin, W. Elsässer and E.O. Göbel, Phys. Rev. A 45 (1992) 1893.
[7] J. Ye, H. Li and J.G. McInerney, Phys. Rev. A 47 (1993) 2249;
H. Li, J. Ye and J.G. McInerney, IEEE J. Quantum Electron. QE-29 (1993) 2421.
[8] A. Ritter and H. Haug, IEEE J. Quantum Electron. QE-29 (1993) 1064.
[9] C. Masoller, A.C. Sicardi Schiffino and C. Cabeza, Optics Comm. 100 (1993) 331.
[10] C. Masoller, Phys. Rev. A 50 No. 2 (1994).
[11] Y. Huang Kao, N. Ming Wang and H. Ming Chen, IEEE J. Quantum Electron. QE-30 (1994) 1732.
[12] T. Sano, Phys. Rev. A 50 (1994) 2719.

[13] C. Masoller, C. Cabeza and A.C. Sicardi Schiffino, IEEE J. Quantum Electron. QE-31 (1995) 1022.
[14] J.D. Farmer, Physica D 4 (1982) 366.
[15] Y. Pomeau, A. Pumir and P. Pelce, J. Stat. Phys. 37 (1984) 39.
[16] K. Ikeda and K. Matsumoto, J. Stat. Phys. 44 (1986) 955; Physica D 29 (1987) 223.
[17] M. Le Berre, E. Ressayre, A. Tallet and H.M. Gibbs, Phys. Rev. Lett. 56 (1986) 274.
[18] B. Dorizzi, B. Grammaticos, M. Le Berre, Y. Pomeau, E. Ressayre and A. Tallet, Phys. Rev. A 35 (1987) 328.
[19] M. Le Berre, E. Ressayre and A. Tallet, Optics Comm. 72 (1989) 123.
[20] F.T. Arecchi, G. Giacomelli, A. Lapucci and R. Meucci, Phys. Rev. A 43 (1991) 4997.
[21] S. Lepri, G. Giacomelli, A. Politi and F.T. Arecchi, Physica D 70 (1993) 235.
[22] G. Giacomelli, R. Meucci, A. Politi and F.T. Arecchi, Phys. Rev. Lett. 73 (1994) 1099.
[23] C. Masoller, unpublished.
[24] H.G. Schuster, Deterministic Chaos, 2nd Ed. (VCH, Weinheim, Germany, 1988).